

# Determination of Local Constitutive Properties of Aluminum using Digital Image Correlation: A Comparative Study Between Uniform Stress and Virtual Fields

**Ali Shahmirzaloo & Mohammadreza Farahani\***

School of Mechanical Engineering,  
College of Engineering, University of Tehran, Tehran, Iran  
E-mail: ali.shahmirzaloo@ut.ac.ir, \*mrfarahani@ut.ac.ir  
\*Corresponding author

**Received: 13 January 2018, Revised: 26 March 2018, Accepted: 10 June 2018**

**Abstract:** A proper understanding of material mechanical properties is important in designing and modelling of components. As a part of a study on the structural integrity, the Digital Image Correlation technique was used to obtain the full-field strain distribution during a tensile test of the specimens. In this study, the elastic and plastic properties of Al6061 alloy has been carried out using both the uniform stress method and the virtual fields method involving digital image correlation technique. In uniform stress methodology, full range stress–strain curves are obtained using the whole field strain measurement using Digital Image Correlation. Recently, the virtual fields method is gaining a lot of popularity in domain characterization as it is robust, accurate and faster. Young's modulus, Poisson's ratio, yield strength, strength coefficient and strain hardening exponent are the parameters extracted using both uniform stress method and virtual fields method. The parameter variation obtained by both uniform stress method and the virtual fields method are compared very well. The Virtual Fields Method provides a theoretically sound basis for developing robust optimization constructs to estimate local material properties, including spatial variations in hardening exponent and strength coefficient. Due to various advantages associated with virtual fields method, it is generally recommended for material mechanical properties extraction.

**Keywords:** Constitutive properties, Digital image correlation, Strain hardening exponent, Strength coefficient introduction, Virtual fields method

**Reference:** Shahmirzaloo, A., and Farahani, M., “Determination of local constitutive properties of aluminium using digital image correlation: A comparative study between uniform stress and virtual fields”, *Int J of Advanced Design and Manufacturing Technology*, Vol. 12/No. 1, 2019, pp. 67-75.

**Biographical notes:** **A. shahmirzaloo** is a master candidate in Mechanical Engineering at University of Tehran, Iran. His current research interest mainly focuses on image processing, Determination of local constitutive properties. **M. Farahani** is associate professor of mechanical engineering at the University of Tehran, Iran. His current research focuses on nondestructive damage sensing and welding engineering using experimental and numerical analysis.

---

## 1 INTRODUCTION

---

A robust method, designated two-dimensional digital image correlation (2D-DIC) was developed in the 1980s [1]-[8]. This method is particularly useful for large deformation measurements. Two-dimensional DIC uses a single scientific grade camera and image correlation software to obtain full-field displacements on nominally planar surfaces, overcoming many of the order method limitations. Once the displacement field is obtained by correlating subsets throughout the images, the 2D surface strain is determined using continuum mechanics and estimated gradients in the surface displacement components. Despite of 2D-DIC advantages relative to other approaches, there are also some limitations in this approach (in 2D DIC), the requirement for intensity interpolation (to increase measurement resolution) introduces small, measurable [9] strain errors under normal laboratory conditions; out-of-plane displacements will affect the accuracy of the image-based measurements, and local shape function will affect the accuracy of the image-based measurements [10].

In recent years, 2-D DIC has been applied to study the heterogeneous material systems [11]-[14]. Lockwood et al. [11], [12] simulated the global response of a friction stir weld using the estimated local constitutive properties as input data for finite element modeling. Their results indicated that USM is a reasonable approximation in their applications. Adeeb et al.[13] used 2D-DIC with the USM to compare the response of transverse and longitudinal specimens across a girth weld, confirming that they behaved similarly under nominally tensile loading. Recently, a methodology based on the principle of virtual work was developed which allows the extraction of simple or more complex analytical models for the constitutive equations of the material. It has been shown that, this method is both efficient and effective when attacking a series of “inverse problems”. The Virtual Fields Method (VFM), has been used with full-field measurements to identify constitutive parameters in homogeneous materials. These studies included (a) linear elastic materials [15]-[18], (b) elastic-plastic material and (c) visco-plastic materials [19]. The method has been shown to be useful and much less time consuming than classical finite element model updating approaches applied to similar problems [20]-[22].

The measurement accuracy of the technique depends on many factors, some of which are related to the algorithms used in correlation calculations [9], [23], [24]. Furthermore, since the technique is based on the tracking of gray level patterns, the accuracy is largely affected by the size of speckles, the image resolution (i.e. number of pixels per speckle) and the chosen subset size in the calculations [25]-[27]. In general, the subset size should be large enough to have a distinctive intensity

pattern. However, the effect of subset size on the accuracy depends on the form of the deformation field to be measured. For relatively homogeneous deformation fields, a large subset size is found to give more accurate displacement measurements, as more data points lead to better correlation [25], [26]. But, when the measured deformation field contains high strain gradients, the variation of the deformation field within a subset can be considerable if the chosen subset size is too large, it can lead to errors if the deformation field is not accurately approximated by subset shape functions [23], [24]. Thus, it seems that smaller subset sizes should be chosen for the measurement of heterogeneous deformation fields. However, the imaging (random) noise becomes more significant with decreasing subset size, which affects the accuracy of the measurement [26], [27]. The choice of subset size also depends on the speckle size. The subset should contain a sufficient number of speckles in order to have a distinctive intensity pattern. Random speckle patterns are usually applied to test surface by various methods, including spray painting. In this work, both the Virtual Fields Method and the Uniform Stress Method are adapted and used to obtain local stress-strain properties of the heterogeneous Al6061 alloy. Hollomon's power law is used as the hardening model for the estimation of plastic parameters of specimen. The parameters extracted in this study are Young's modulus, Poisson's ratio, yield stress, strength coefficient and hardening exponent.

---

## 2 INTRODUCTION TO DIGITAL IMAGE CORRELATION (DIC)

---

DIC is a versatile non-contact optical technique that came into popularity from 1980s [1], [2]. It is used as a reliable tool in experimental mechanics to obtain whole field displacement and strain fields. It is based on image comparison of the specimens coated with a random speckle pattern. Speckle patterns are nothing but random black dots sprayed over the specimen painted with white paint. The speckle pattern of the undeformed specimen (reference image) is compared with the images of deformed specimen and using pattern matching principles, displacements are computed. Since it is not practical to compare each pixel in the image, a small area containing multiple pixels called subsets are traced relatively. The pattern matching is based on obtaining maximum correlation between subsets of the image in the undeformed and deformed states (see Fig. 1 [28]). A correlation function is used for matching purposes as shown in Eq. (1) [28]. The displacement of the center of pixel subset is returned when a best match is identified. The strain fields are obtained from the gradients of smoothed displacement fields using a numerical differentiation scheme using below equation.

$$C(u, v) = \frac{\sum_{i=1}^m \sum_{j=1}^m [f(x_i, y_i) - \bar{f}][g(x'_i, y'_i) - \bar{g}]}{\sqrt{\sum_{i=1}^m \sum_{j=1}^m [f(x_i, y_i) - \bar{f}]^2} \sqrt{\sum_{i=1}^m \sum_{j=1}^m [g(x'_i, y'_i) - \bar{g}]^2}} \quad (1)$$

Where

$$x' = x + u_0 + \frac{\partial u}{\partial x} dx + \frac{\partial u}{\partial y} dy \quad (2)$$

$$y' = y + v_0 + \frac{\partial v}{\partial x} dx + \frac{\partial v}{\partial y} dy \quad (3)$$

$\bar{f}$  is the mean intensity value of reference subset,  $\bar{g}$  is the mean intensity value of deformed subset,  $m$  is the width of subset in pixels and  $u_0, v_0$  are translations of the centre of the subset in the  $x$  and  $y$  directions.

In a 2D DIC setup, one camera is used for image grabbing. This system is capable of measuring in-plane surface displacements and strains, whereas 3D DIC setup has got two cameras for simultaneous image grabbing and utilizes a detailed calibration procedure to synchronize the camera coordinates and image location. Upon calibration of a 3D DIC system, the sensor plane locations in the two views for the same object point can be used to determine an accurate estimate of the three-dimensional position of the common object location [29]. In case of 3D DIC, one can get out-of-plane displacement in addition to in plane displacement and strain. For more details on the development and capability of DIC, readers are advised to refer the following literatures [30]-[35].

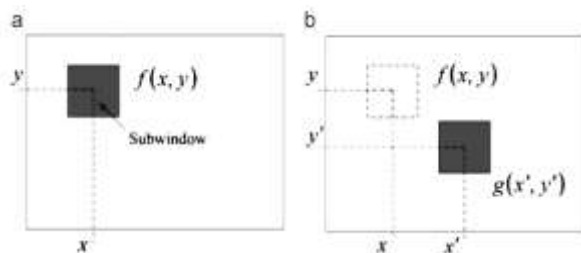


Fig. 1 Schematic of subset matching in DIC, (a) Unreformed and (b) deformed

### 3 VIRTUAL FIELDS FORMULATION

In this section, the basic equations and methodology used for solving elastic and plastic parameters using VFM are discussed in detail. Fig. 2 [36] shows the free body diagram of the tensile test specimen containing the displacement and force boundary conditions. Area of interest (AOI) in the figure is this area over which the strain values are known.

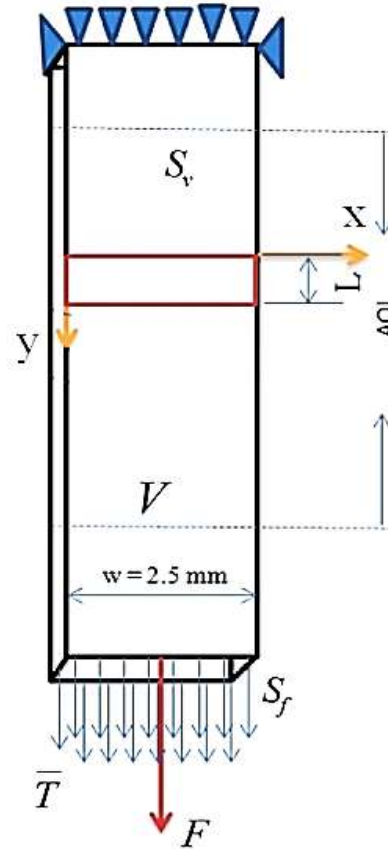


Fig. 2 Diagram showing the loading and boundary conditions of the tensile testing

The known parameters from the tensile test are the reaction force  $F$ , surface strain distribution over the specimen and the displacement prescribed over  $S_u$ . The basic governing equation of VFM is given in Eq. (4) [36]. This equation is nothing but the weak form of the equilibrium equation derived using the principle of virtual work.

$$\int_V \sigma_{ij} : \varepsilon_{ij}^* dv + \int_{S_f} \bar{T}_i \cdot u_i^* ds + \int_V b_i \cdot u_i^* dv = \int_V \rho a_i \cdot u_i^* dv \quad (4)$$

Where

$V$ : is the volume of the element.

$S_U$ : is the area ( $x$ - $y$  plane) where the surface strain data is measured using DIC.

$S_f$ : is the area where traction boundary condition is applied

$\sigma_{ij}$ : is the stress tensor.

$u_i^*$ : is the virtual displacement field which is kinematically admissible.

$\varepsilon_{ij}^*$ : is the virtual strain tensor derived from virtual displacement field.

$b_i$ : is the volume force vector.

$a_i$ : is the acceleration vector

$\rho$ : is the density of the material

Since the volume and inertia forces have negligible contribution towards the total work done, Eq. (4) can be simplified as given below:

$$\int_V \sigma_{ij} : \varepsilon_{ij}^* dv = \int_{S_f} \bar{T}_i \cdot u_i^* ds \quad (5)$$

In a plane stress condition where a two-dimensional stress state exists with the assumption that there is no variation in the stress state along the thickness direction, one can rewrite Eq. (5) as given in Eq. (6). Here  $b$  is the thickness of the specimen.

$$b \int_{S_v} \sigma_{ij} : \varepsilon_{ij}^* dS_v = b \int_w \bar{T}_i \cdot u_i^* dw \quad (6)$$

Also, one gets reaction force  $F$  corresponding to load step  $t_i$  in terms of traction as given below:

$$b \int_w \bar{T}_i dw = F(t_i) \quad (7)$$

On substitution of Eq. (7) in Eq. (6), one gets:

$$\int_{S_v} \sigma_{ij} : \varepsilon_{ij}^* dS_v = \frac{1}{b} F(t_i) \cdot u_i^* \quad (8)$$

The above equation is the simplified form of VFM which is used in this study for elastic and plastic parameter identification.

### 3.1 ELASTIC PARAMETER IDENTIFICATION

To extract two elastic constants namely Young's modulus and Poisson's ratio, Eq. (8) was utilized. The known quantities from the tensile test are the strain over the surface  $S_v$  and reaction load  $F(t_i)$ . In order to introduce the unknown parameters and actual strain measured using a DIC technique into Eq. (8), the stress

tensor is replaced with the constitutive relation given in Eq. (9) [36]. Note that a plane stress assumption is employed and the strain  $\varepsilon_{ij}$  is the actual strains measured over the surface  $S_v$  using DIC technique.

$$\begin{bmatrix} \sigma_{xx} \\ \sigma_{yy} \\ \sigma_{xy} \end{bmatrix} = \begin{bmatrix} \frac{E}{1-\nu^2} & \frac{\nu E}{1-\nu^2} & 0 \\ \frac{\nu E}{1-\nu^2} & \frac{E}{1-\nu^2} & 0 \\ 0 & 0 & \frac{E}{1+\nu} \end{bmatrix} \begin{bmatrix} \varepsilon_{xx} \\ \varepsilon_{yy} \\ \varepsilon_{xy} \end{bmatrix} \quad (9)$$

Now Eq. (8) can be expanded to the form given in Eq. (10). This equation contains the unknown variables, actual strains measured over the surface  $S_v$ , reaction force  $F(t_i)$ , virtual strains and virtual displacements. It is clear that this equation should satisfy for any kinematically admissible selection of virtual displacement fields. Kinematically admissible means the field which continues and satisfies displacement boundary conditions.

$$\begin{aligned} & \frac{E}{1-\nu^2} \left( \int_{S_v} \varepsilon_{xx} \varepsilon_{xx}^* dS_v + \int_{S_v} \varepsilon_{yy} \varepsilon_{yy}^* dS_v \right) \\ & + \frac{\nu E}{1-\nu^2} \left( \int_{S_v} \varepsilon_{xx} \varepsilon_{yy}^* dS_v + \int_{S_v} \varepsilon_{yy} \varepsilon_{xx}^* dS_v \right) \\ & + \frac{E}{1+\nu} \left( \int_{S_v} \varepsilon_{xy} \varepsilon_{xy}^* dS_v \right) = \frac{1}{b} F(t_i) \cdot u_i^* \end{aligned} \quad (10)$$

Since the strain distribution from DIC technique is not a continuous function over the surface, but they are valued at discrete points called pixel subset center, above equation can be rewritten as a summation over the surface as given below. Here,  $N$  is the number of data points on the area of the zone under consideration.

$$\begin{aligned} & \frac{E}{1-\nu^2} \left( \frac{1}{N} \sum_{i=1}^N \varepsilon_{xx} \varepsilon_{xx}^* \Delta S_v \right. \\ & \quad \left. + \frac{1}{N} \sum_{i=1}^N \varepsilon_{yy} \varepsilon_{yy}^* \Delta S_v \right) \\ & + \frac{\nu E}{1-\nu^2} \left( \frac{1}{N} \sum_{i=1}^N \varepsilon_{xx} \varepsilon_{yy}^* \Delta S_v \right. \\ & \quad \left. + \frac{1}{N} \sum_{i=1}^N \varepsilon_{yy} \varepsilon_{xx}^* \Delta S_v \right) \\ & + \frac{E}{1+\nu} \left( \frac{1}{N} \sum_{i=1}^N \varepsilon_{xy} \varepsilon_{xy}^* \Delta S_v \right) = \frac{1}{b} F(t_i) \cdot u_i^* \end{aligned} \quad (11)$$

Selection of two independent virtual displacement fields will result in two linear independent equations. The

unknown parameters (E and  $\nu$ ) can be extracted by solving this system of equations. Virtual fields used in this study are defined below. A graphical representation of the virtual field selected is depicted in Fig. 3, where the virtual deformation is superimposed on the undeformed configuration.

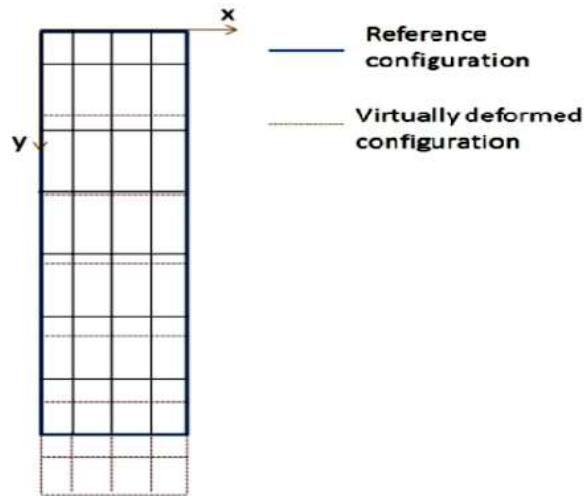


Fig. 3 The virtual displacement fields

Virtual field is selected in such a way that the material apart from the zone under consideration behaves like a rigid body so that they have no contribution towards internal virtual work. Refer Fig. 2 for the schematic diagram showing zone of dimension L. Virtual field [36]:

$$\begin{aligned} u_{x1}^* &= 0 \text{ and } u_{y1}^* = 0 \text{ for } y < 0 \\ u_{x1}^* &= 0 \text{ and } u_{y1}^* = y \text{ for } 0 < y < L \\ u_{x1}^* &= 0 \text{ and } u_{y1}^* = 0 \text{ for } y \geq L \end{aligned} \quad (12)$$

Corresponding virtual strain fields are [36]:

$$\begin{aligned} \varepsilon_{xx}^* &= 0, \varepsilon_{yy}^* = 0 \text{ and } \varepsilon_{xy}^* = 0 \text{ for } y < 0 \\ \varepsilon_{xx}^* &= 0, \varepsilon_{yy}^* = 1 \text{ and } \varepsilon_{xy}^* = 0 \text{ for } 0 < y < L \\ \varepsilon_{xx}^* &= 0, \varepsilon_{yy}^* = 0 \text{ and } \varepsilon_{xy}^* = 0 \text{ for } y \geq L \end{aligned} \quad (13)$$

Substituting virtual field in Eq. (11) we will get the equation as shown below. Also note that here  $\Delta S_v$  is the area of the zone under consideration:

$$\begin{aligned} \frac{E}{1-\nu^2} \left( \frac{1}{N} \sum_{i=1}^N \varepsilon_{yy} \right) \Delta S_v \\ + \frac{\nu E}{1-\nu^2} \left( \frac{1}{N} \sum_{i=1}^N \varepsilon_{xx} \right) \Delta S_v \end{aligned} \quad (14)$$

$$= \frac{1}{b} F(t_i) \cdot L$$

### 3.2 PLASTIC PARAMETER IDENTIFICATION

Since the strain evolution upon loading is non-linear in the plastic deformation region, it is not possible to extract the required parameters from a single strain and load data as in the case of elasticity involving VFM. At various load levels this nonlinearity will rise to independent system of equations even against a single chosen virtual displacement field. This property is used by Grédiac et al. [36] for formulating a minimization problem to extract the plastic constitutive parameters. Here, in order to solve for the unknown material parameters, the virtual displacement field given in Eq. (12) is used. Upon substitution of this virtual displacement and corresponding virtual strains in Eq. (8) one gets Eq. (15) as shown below:

$$\int_{S_v} \sigma_{ij} dS_v = \frac{1}{b} F(t_i) \cdot L \quad (15)$$

Now by replacing  $\sigma_{ij}$  with the material model given in  $\sigma_{yy} = K(\varepsilon_{yy} - (\frac{\sigma_{ys}}{E}))^n$ , one can rewrite Eq. (15) as given below

$$\int_{S_v} K(\varepsilon_{yy} - (\frac{\sigma_{ys}}{E}))^n dS_v = \frac{1}{b} F(t_i) \cdot L \quad (16)$$

Eq. (17) is obtained by changing the integration operation in Eq. (16) to summation over the area where N is the number of measurement points in the zone under consideration:

$$\frac{1}{N} \sum_{i=1}^N K(\varepsilon_{yy} - (\frac{\sigma_{ys}}{E}))^n \Delta S_v = \frac{1}{b} F(t_i) \cdot L \quad (17)$$

The known parameters in the above equation are E obtained from the elastic analysis, N,  $\varepsilon_{yy}$ ,  $\Delta S_v$ ,  $F(t_i)$ , L and b. In order to solve for the unknown values (K, n and  $\sigma_{ys}$ ), a cost function is developed as shown below.

$$f = \sum_{t_1}^{t_n} \left[ \frac{1}{N} \sum_{i=1}^N K(\varepsilon_{yy} - (\frac{\sigma_{ys}}{E}))^n \Delta S_v - \frac{1}{b} F(t_i) \cdot L \right]^2 \quad (18)$$

Where  $t_1, t_2 \dots t_n$  are the load steps selected in the plastic deformation region.

#### 4 EXPERIMENTAL PROCEDURE

The material used for this study was 2mm-thick sheets of 6061 aluminum alloys. The specimen was machined from a 6061 aluminum alloy rolled plate using electro discharge machining (EDM) as shown in Figure 4. It had a gauge length of 32 mm, width of 5 mm and thickness of 2mm.

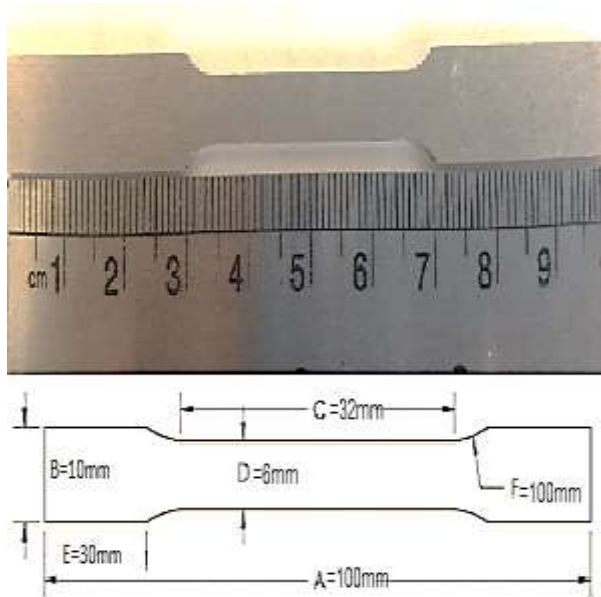


Fig. 4 The tensile specimen and its dimensions



Fig. 5 Two different speckle patterns on the specimens

All tensile tests were performed on a 30-kN servo hydraulic test machine operated in ram-displacement control. To obtain correctable images, a high contrast

pattern must be applied to the considered surface. A white spray-painted background with a black overspray provides the necessary contrast in the images as shown. In Fig. 5, two different speckle pattern were used in order to achieve an acceptable correlation coefficient. A digital imaging camera (DMK 33UX264), with a sensor size of 2,448×2,048 pixels (5 Mega Pixels), and a 75 mm macro lens was used to capture images at each load level. In this study, 60 images are grabbed every minute. The load value corresponding to each image was reached. The images were analyzed using DIC software to obtain displacement maps at various parameter settings. The displacement data were then used to calculate the axial strain ( $\epsilon_y$ ) variation.

#### 5 RESULTS AND DISCUSSIONS

In the primary studies, sensitivity analysis performed for studying the influence of DIC subset size on the correlation coefficient is discussed. Since the technique is based on the tracking of gray level patterns, the accuracy is largely affected by the size of speckles, the image resolution (i.e. number of pixels per speckle) and the chosen subset size in the calculations. For specimen with tiny speckle pattern, effect of subset size was investigated on the correlation coefficient. According to Fig. 6, suitable value for subset size equal to 45 pixels is selected for further image processing.

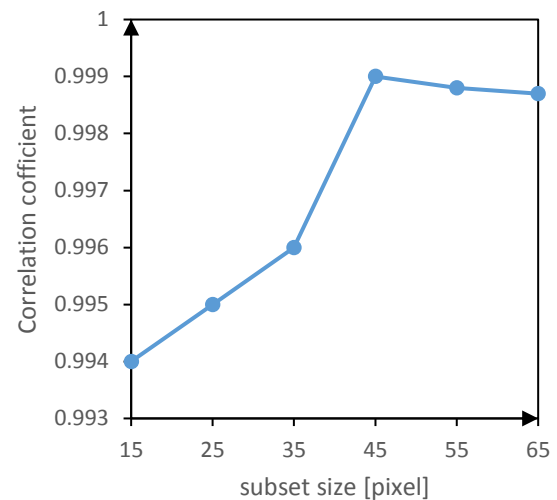


Fig. 6 Analysis on effect speckle pattern on correlation coefficient

Fig. 7 shows the surface strain distribution obtained at various load levels in a tensile test. As can be seen, the strain growth around the failure zone was detectable.

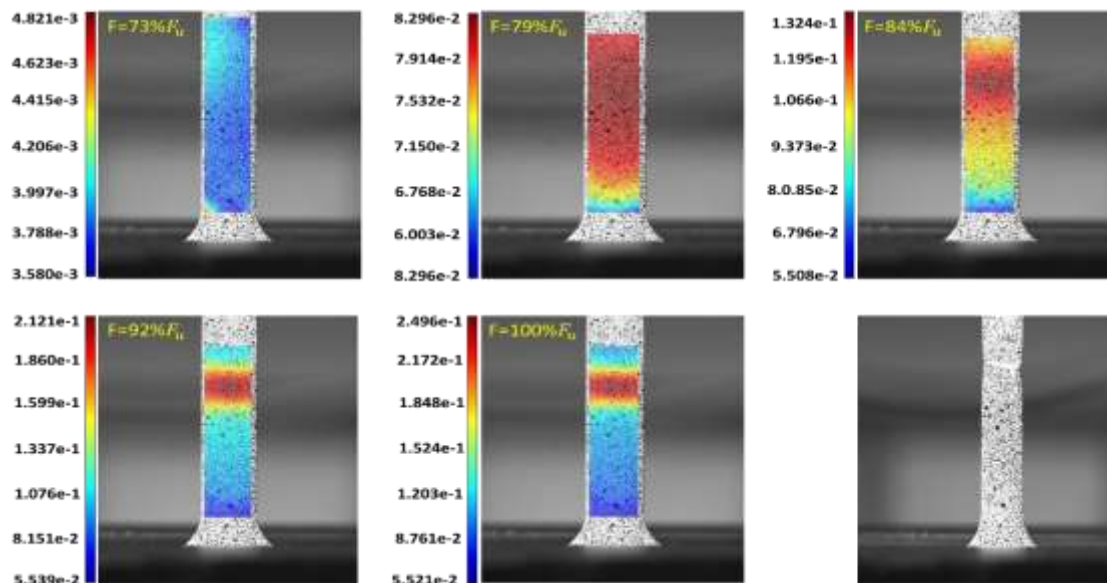


Fig. 7 Longitudinal strain distribution at various load levels

Base on stress-strain diagram slope, the Young's modulus can be obtained. In Fig 8, the stress-strain curve obtained from DIC and tension test are compared as can be seen, the diagram slope (Young's modulus) from tension test shows an unacceptable value. Also according to the strain values in (x, y) direction, Poisson coefficient can be calculated.

Fig. 8 represents the engineering stress-strain behavior of the specimen. Using the homogeneous stress assumption, the local stress–strain response of a heterogeneous material undergoing nominally tension loading is given by the stress–strain pairs as blows [37].

$$\left\{ \frac{F(t_i)}{Dt}, \varepsilon_{yy} \right\} \quad (19)$$

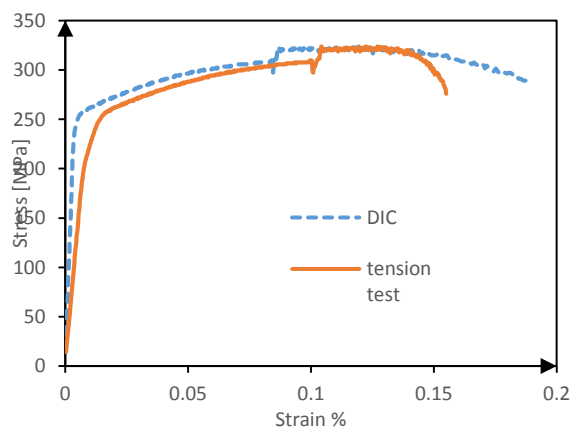


Fig. 8 Engineering stress-strain variation obtained by two different methods

Young's modulus values obtained from DIC and tension test were given in Table 1. As the Poisson's ratio value could not be measured by the simple tension test, its value is only provided by means of DIC.

Table 1 Elastic properties values obtained from DIC and tension test

Elastic properties	DIC	Tension test
Young's modulus	70.4 GPa	25 GPa
Poisson's ratio	0.314	-

The stress–strain curves obtained using DIC are utilized for determining the limit between the elastic and plastic regions. The linear zone and the corresponding load levels can easily be identified from the stress–strain curve. For finding the starting point of plastic zone, 0.2% offset yield strength is estimated from the stress–strain curve and consequently the load and deformation values registered after this point are categorized as plastic zone. Parameter extraction using USM is carried out by fitting the material model as shown in Eq20 onto the experimental curves. Using MATLAB and data fitting on DIC data, plastic mechanical properties are obtained as shown in the table.2.

$$\sigma = k\varepsilon^n \quad (20)$$

Table 2 Plastic properties obtained using USM

Plastic properties	Value
Strength coefficient(k)	460 MPa
Strain hardening exponent(n)	0.0869

For the examined specimen, Eq. (14) is solved by feeding known surface strain values from DIC technique and reaction load value from the load cell. Minimization of the cost function given in Eq. (18) results in the direct identification of the unknown parameters. In this study, a derivative free multi-variable optimization scheme, Nelder–Mead algorithm [38] is used for solving the equation. Nelder–Mead algorithm, also known as the downhill simplex method, is a technique for minimizing an objective function in a many dimensional space. It requires an initial guess to start with. Even though any reasonable initial guess will result in consistent results, in this study the parameters close to material properties are chosen as the initial guess. It can result in faster convergence. Optimization toolbox in MATLAB is utilized for the minimization process. Young's modulus, Poisson's ratio, strength coefficient (k) and strain hardening exponent (n) bases on Grédiac equation were extracted using VFM as reported in Table 3.

**Table 3** Constitutive material properties extracted using VFM

Constitutive properties	Value
Young's modulus	74.3
Poisson's ratio	0.305
strength coefficient	680
hardening exponent	.0582

## 6 CONCLUSIONS

Two methods have been used to obtain local stress–strain behavior in a specimen undergoing nominally uniaxial tension load. Results show that the Virtual Fields Method provides a theoretically sound basis for developing robust optimization constructs to estimate local material properties, including spatial variations in hardening exponent and strength coefficient. It offers a significant improvement in the spatial resolution and enables the determination of plastic parameters over local areas. Using the DIC base technique, material behavior can be determined from any or all points in the specimen region with a spatial resolution limited only by the usable magnification of the imaging system and the ability to apply a pattern of appropriate scale. Meanwhile, no prior knowledge of material properties is required (e.g. as in automated ball indentation tests). VFM has clear advantages over USM in material characterization. In VFM there is no requirement of stresses to be constant in the cross-section. Further, only fewer images are required for the material parameter extraction and full range stress–strain curve as required for USM are not necessary.

## REFERENCES

- [1] Peters, W., Ranson, W., "Digital Imaging Techniques in Experimental Stress analysis", *Optical engineering*, Vol. 21, No. 3, 1982, pp. 213427-213427.
- [2] Sutton, M., Wolters, W., Peters, W., Ranson, W., and McNeill, S., "Determination of Displacements Using an Improved Digital Correlation Method", *Image and vision computing*, Vol. 1, No. 3, 1983, pp. 133-139.
- [3] He, Z., Sutton, M., Ranson, W., and Peters, W., "Two-Dimensional Fluid-Velocity Measurements by Use of Digital-Speckle Correlation Techniques", *experimental mechanics*, Vol. 24, No. 2, 1984, pp. 117-121.
- [4] Chu, T., Ranson, W., and Sutton, M. A., "Applications of Digital-Image-Correlation Techniques to Experimental Mechanics", *Experimental mechanics*, Vol. 25, No. 3, 1985, pp. 232-244.
- [5] Sutton, M., Mingqi, C., Peters, W., Chao, Y., and McNeill, S., "Application of an Optimized Digital Correlation Method to Planar Deformation Analysis", *Image and Vision Computing*, Vol. 4, No. 3, 1986, pp. 143-150.
- [6] Sutton, M. A., McNeill, S. R., Jang, J., and Babai, M., "Effects of Subpixel Image Restoration on Digital Correlation Error Estimates", *Optical Engineering*, Vol. 27, No. 10, 1988, pp. 271070-271070.
- [7] Sutton, M., Bruck, H., and McNeill, S., "Determination of Deformations Using Digital Correlation with the Newton-Raphson Method for Partial Differential Corrections", *Exp Mech*, Vol. 29, No. 3, 1989, pp. 261-267.
- [8] Sutton, M. A., Chae, T. L., Turner, J. L., and Bruck, H. A., "Development of a Computer Vision Methodology for the Analysis of Surface Deformations in Magnified Images", *MiCon 90: Advances in Video Technology for Microstructural Control*, ASTM International, Philadelphia, 1991.
- [9] Schreier, H. W., Braasch, J. R., and Sutton, M. A., "Systematic Errors in Digital Image Correlation Caused by Intensity Interpolation", *Optical engineering*, Vol. 39, No. 11, 2000, pp. 2915-2921.
- [10] Schreier, H., Sutton, M., "Effect of Higher Order Displacement Fields on Digital Image Correlation Displacement Component Estimates", *Exp Mech*, Vol. 42, No. 3, 2002, pp. 303-311.
- [11] Lockwood, W. D., Tomaz, B., and Reynolds, A. P., "Mechanical Response of Friction Stir Welded AA2024: Experiment and Modeling", *Materials Science and Engineering: A*, Vol. 323, No. 1, 2002, pp. 348-353.
- [12] Lockwood, W., Reynolds, A. P., "Simulation of the Global Response of a Friction Stir Weld Using Local Constitutive Behavior", *Materials Science and Engineering: A*, Vol. 339, No. 1, 2003, pp. 35-42.
- [13] Lagattu, F., Brillaud, J., and Lafarie-Frenot, M. C., "High Strain Gradient Measurements by Using Digital Image Correlation Technique", *Materials characterization*, Vol. 53, No. 1, 2004, pp. 17-28.
- [14] Adeeb, S., Horsley, D., Yan, J., Sutton, M. A., and Reynolds, A. P., "Local Stress-Strain Response of an

- Axial X100 Girth Weld Under Tensile Loading Using Digital Image Correlation”, 2006 International Pipeline Conference: American Society of Mechanical Engineers, 2006, pp. 339-348.
- [15] Grédiac, M. “Principe Des Travaux Virtuels et Identification”, Comptes rendus de l'Académie des sciences Série 2, Mécanique, Physique, Chimie, Sciences de l'univers, Sciences de la Terre, Vol. 309, No. 1, 1989, pp. 1-5.
- [16] Grédiac, M., Toussaint, E., and Pierron, F., “Special Virtual Fields for the Direct Determination of Material Parameters with the Virtual Fields Method. 1–Principle and Definition”, International Journal of Solids and Structures, Vol. 39, No. 10, 2002, pp. 2691-2705.
- [17] Grediac, M., Pierron, F., Avril, S., and Toussaint, E., “The Virtual Fields Method for Extracting Constitutive Parameters from Full-Field Measurements: a Review”, Strain, Vol. 42, No. 4, 2006, pp. 233-253.
- [18] Avril, S., Pierron, F., “General Framework for the Identification of Constitutive Parameters from Full-Field Measurements in Linear Elasticity”, International Journal of Solids and Structures, Vol. 44, No. 14, 2007, pp. 4978-5002.
- [19] Avril, S., Pierron, F., Yan, J., and Sutton, M. A., “Identification of Viscoplastic Parameters Using DIC and the Virtual Fields Method”, Proceedings of the SEM Conference and Exposition, Springfield, USA, 2007.
- [20] Meuwissen, M., Oomens, C., Baaijens, F., Pettersson, R., and Janssen, J. D., “Determination of the Elasto-Plastic Properties of Aluminium Using a Mixed Numerical–Experimental Method”, Journal of Materials Processing Technology, Vol. 75, No. 1, 1998, pp. 204-211.
- [21] Kajberg, J., Lindkvist, G., “Characterisation of Materials Subjected to Large Strains by Inverse Modelling Based on In-Plane Displacement Fields”, International Journal of Solids and Structures, Vol. 41, No. 13, 2004, pp. 3439-3459.
- [22] Kajberg, J., Wikman, B., “Viscoplastic Parameter Estimation by High Strain-Rate Experiments and Inverse Modelling–Speckle Measurements and High-Speed Photography”, International Journal of Solids and Structures, Vol. 44, No. 1, 2007, pp. 145-164.
- [23] Schreier, H. W., Sutton, M. A., “Systematic Errors in Digital Image Correlation Due to Undermatched Subset Shape Functions”, Experimental Mechanics, Vol. 42, No. 3, 2002, pp. 303-310.
- [24] Bing, P., Hui-Min, X., Bo-Qin, X., and Fu-Long, D., “Performance of Sub-Pixel Registration Algorithms in Digital Image Correlation”, Measurement Science and Technology, Vol. 17, No. 6, 2006, pp. 1615.
- [25] Lecompte, D., Smits, A., Bossuyt, S., Sol, H., Vantomme, J., Van Hemelrijck, D., and Habraken, A., “Quality Assessment of Speckle Patterns for Digital Image Correlation”, Optics and lasers in Engineering, Vol. 44, No. 11, 2006, pp. 1132-1145.
- [26] Yaofeng, S., Pang, J. H., “Study of Optimal Subset Size in Digital Image Correlation of Speckle Pattern Images”, Optics and lasers in engineering, Vol. 45, No. 9, 2007, pp. 967-974.
- [27] Pan, B., Xie, H., Wang, Z., Qian, K., and Wang, Z., “Study on Subset Size Selection in Digital Image Correlation for Speckle Patterns”, Optics express, Vol. 16, No. 10, 2008, pp. 7037-7048.
- [28] Saranath, K., Sharma, A., and Ramji, M., “Zone Wise Local Characterization of Welds Using Digital Image Correlation Technique”, Optics and Lasers in Engineering, Vol. 63, 2014, pp. 30-42.
- [29] Sutton, M., Yan, J., Tiwari, V., Schreier, H., and Orteu, J., “The Effect of Out-of-Plane Motion on 2D and 3D Digital Image Correlation Measurements”, Optics and Lasers in Engineering, Vol. 46, No. 10, 2008, pp. 746-757.
- [30] Sutton, M. A., Orteu, J. J., and Schreier, H., “Image Correlation for Shape, Motion and Deformation Measurements: Basic Concepts, Theory and Applications”, Springer Science & Business Media, New York, 2009.
- [31] Rao, R. V., “Advanced Modeling and Optimization of Manufacturing Processes: International Research and Development”, Springer Science & Business Media, New York, 2010.
- [32] Hu, Z., Xie, H., Lu, J., Wang, H., and Zhu, J., “Error Evaluation Technique for Three-Dimensional Digital Image Correlation”, Applied optics, Vol. 50, No. 33, 2011, pp. 6239-6247.
- [33] Reu, P., “A Study of the Influence of Calibration Uncertainty on the Global Uncertainty for Digital Image Correlation Using a Monte Carlo Approach”, Experimental Mechanics, Vol. 53, No. 9, 2013, pp. 1661-1680.
- [34] Yang, R. c., “A Regularized Finite-Element Digital Image Correlation for Irregular Displacement Field”, Optics and Lasers in Engineering, Vol. 56, 2014, pp. 67-73.
- [35] Zhou, Y., Sun, C., and Chen, J., “Adaptive Subset Offset for Systematic Error Reduction in Incremental Digital Image Correlation”, Optics and Lasers in Engineering, Vol. 55, 2014, pp. 5-11.
- [36] Saranath, K., Ramji, M., “Local Zone Wise Elastic and Plastic Properties of Electron Beam Welded Ti–6Al–4V Alloy Using Digital Image Correlation Technique: A Comparative Study Between Uniform Stress and Virtual Fields Method”, Optics and Lasers in Engineering, Vol. 68, 2015, pp. 222-234.
- [37] Sutton, M., Yan, J., Avril, S., Pierron, F., and Adeeb, S., “Identification of Heterogeneous Constitutive Parameters in a Welded Specimen: Uniform Stress and Virtual Fields Methods for Material Property Estimation”, Experimental Mechanics, Vol. 48, No. 4, 2008, pp. 451-464.
- [38] Nelder, J. A., Mead, R., “A Simplex Method for Function Minimization”, The computer journal, Vol. 7, No. 4, 1965, pp. 308-31